

Ambient Species Density and Gas Temperature Radial Profiles Derived from a Schlieren Technique in a Low-Frequency Non-thermal Oxygen Plasma Jet

J. C. Chamorro¹ · L. Prevosto¹ · E. Cejas¹ · G. Fischfeld² ·
H. Kelly¹ · B. Mancinelli¹

Received: 12 May 2017 / Accepted: 29 August 2017
© Springer Science+Business Media, LLC 2017

Abstract A quantitative interpretation of the schlieren technique applied to a non-thermal atmospheric-pressure oxygen plasma jet driven at low-frequency (50 Hz) is reported. The jet was operated in the turbulent regime with a hole-diameter based Reynolds number of 13,800. The technique coupled to a simplified kinetic model of the jet effluent region allowed deriving the temporally-averaged values of the gas temperature of the jet by processing the gray-level contrast values of digital schlieren images. The penetration of the ambient air into the jet due to turbulent diffusion was taken into account. The calibration of the optical system was obtained by fitting the sensitivity parameter so that the oxygen fraction at the nozzle exit was unity. The radial profiles of the contrast in the discharge off case were quite symmetric on the whole outflow, but with the discharge on, relatively strong departures from the symmetry were evident in the near field. The time-averaged gas temperature of the jet was relatively high, with a maximum departure of about 55 K from the room temperature; as can be expected owing to the operating molecular gas. The uncertainty in the temperature measurements was within 6 K, primarily derived from errors associated to the Abel inversion procedure. The results showed an increase in the gas temperature of about 8 K close to the nozzle exit; thus suggesting that some fast-gas heating (with a heating rate ~ 0.3 K/ μ s) still occurs in the near field of the outflow.

Keywords Non-equilibrium plasma jet · Gas temperature · Turbulent air mixing · Schlieren technique

✉ L. Prevosto
prevosto@waycom.com.ar

¹ Grupo de Descargas Eléctricas, Departamento Ing. Electromecánica, Facultad Regional Venado Tuerto (UTN), Laprida 651, 2600 Venado Tuerto, Santa Fe, Argentina

² Facultad de Ciencias Exactas, Ingeniería y Agrimensura (UNR), Pellegrini 250, 2000 Santa Fe, Argentina

Introduction

Nowadays a very active field in plasma physics is the development of non-thermal plasma sources [1, 2]. Typical sources for atmospheric-pressure non-thermal plasmas include corona discharges; dielectric barrier discharges, and glows (with or without a superimposed gas flow) [3–5]. The non-equilibrium state is characterized by the presence of energetic electrons, that produce in turn ions and highly active chemical reactive species, but without the generation of excessive heat which could damage substrates (typically the gas temperature in the effluent is less than 100 °C). Owing to these features, non-thermal plasmas have found widespread use in a variety of industrial applications such as pollution control applications, volatile organic compounds removal, car exhaust emission control and polymer surface treatment (to promote wettability, printability and adhesion) [4, 5]; and more recently (for sub—60 °C plasmas); also in plasma biology and plasma medicine [1, 6, 7]. For decades, non-thermal plasmas have been used to generate ozone for water purification [5].

Among different kind of non-thermal atmospheric-pressure plasma sources, low-current (~ 0.1 A) plasma jets have rapidly gained importance in various plasma processing applications (including biomedical applications) because they can operate in open air providing plasmas without spatial confinement [5, 8–11]. An afterglow containing electrons, ions and relative long-lifetime radicals dragged from the confined discharge by a relatively large gas flow; is formed at the outflow of those sources. The gas temperature largely depends on the gas type. It increases with the number of internal energy modes (e.g., molecular gases), and decrease with increased thermal conductivity. A variety of plasma jets using quasi-stationary (low-frequency) or pulsed power sources operating at quite different voltages, frequencies, and pulse widths, and with different working gases have been reported in the literature (see for instance [1] and references therein).

Consequently, a proper knowledge on the gas temperature and mixing level with the ambient air due to diffusive particle fluxes into the afterglow becomes important not only for the plasma processing application, but also for understanding basic chemical mechanisms in non-thermal plasma jets. Optical methods represent a versatile tool for performing non-intrusive, quantitative measurements in transparent media [12]. In particular; refractive techniques allow the investigation of the gas density distribution in transparent flows by measuring its index of refraction (or its spatial derivatives). These refractive techniques can be divided into two groups: the interference methods, based on the difference in length of the light ray paths, and the methods based on the angular deflections of the light rays, such as shadowgraph and schlieren. The schlieren technique is based on the angular deflection undergone by a light ray when passing through a region characterized by refractive index non-homogeneities. In fluids, these non-homogeneities are generally caused by density or temperature variations; therefore the measured optical data can be processed in order to gain information on such variables. An extensive description of the schlieren technique can be found elsewhere [13, 14].

A relative large number of papers have been devoted to qualitatively investigate the plasma flow and its interaction with the ambient air (mainly fluid dynamics characteristics) in a variety of non-thermal plasma jets by using schlieren images [15–23]. For plasma sources operated at higher temperatures, as nanosecond repetitively pulsed discharges [24], flames [25] and thermal arcs [26–28]; also quantitative schlieren techniques have been used to determine the gas temperature and plasma composition. However, quantitative data from schlieren images in non-thermal plasma jets are very scarce. Only recently, a quantitative schlieren diagnostic in a non-thermal atmospheric-pressure argon plasma jet

driven at high-frequency (~ 0.9 MHz) was reported [29]. It was found that the change of the index of refraction due to the mixing of argon and air is of the same order of magnitude as the change due to the gas temperature variations.

In this work, a quantitative interpretation of the schlieren technique applied to a non-thermal atmospheric-pressure oxygen plasma jet driven at low-frequency (50 Hz) is reported. The technique allowed measuring the temporally-averaged values of the gas temperature of the fully turbulent jet by processing the gray-level contrast values of a digital schlieren image recorded at the observation plane for a given position of a transverse knife-edge located at the exit focal plane of the optical system. To the best of the author's knowledge neither experimental nor numerical investigations on non-thermal atmospheric-pressure plasma jets operating with pure oxygen as the feed gas have yet been reported.

Experimental Arrangement

Non-thermal Plasma Source

The experiments were carried out using a non-thermal atmospheric-pressure plasma jet. The device consisted in two coaxial electrodes through which the gas flows axially. The outer (grounded) electrode (i.e., the nozzle) was made of aluminum with a hole of 1 mm diameter; while the inner (rod-type) electrode was made of copper. The jet was driven at low-frequency (50 Hz). Dry oxygen (O_2 purity in excess of 99.5%) was used as the feed gas at a (measured) gas flow rate of 10 Nl min^{-1} . A scheme of the device indicating several geometric dimensions is shown in Fig. 1. When the discharge was turned on, the visible plasma jet had a typical length < 10 mm.

The ac power supply was a high-voltage transformer (25 kV, 100 mA, and 50 Hz) with a high-dispersion reactance (75 ± 0.5 k Ω) connected to a variable autotransformer to control the discharge current. The electric circuit used to generate the atmospheric pressure non-thermal plasma jet is also presented schematically in Fig. 1. Because of the high-impedance of the transformer provides an intrinsic current limitation, the use of external

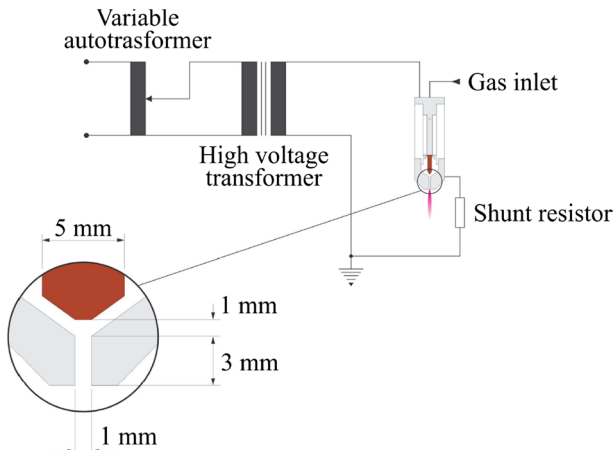
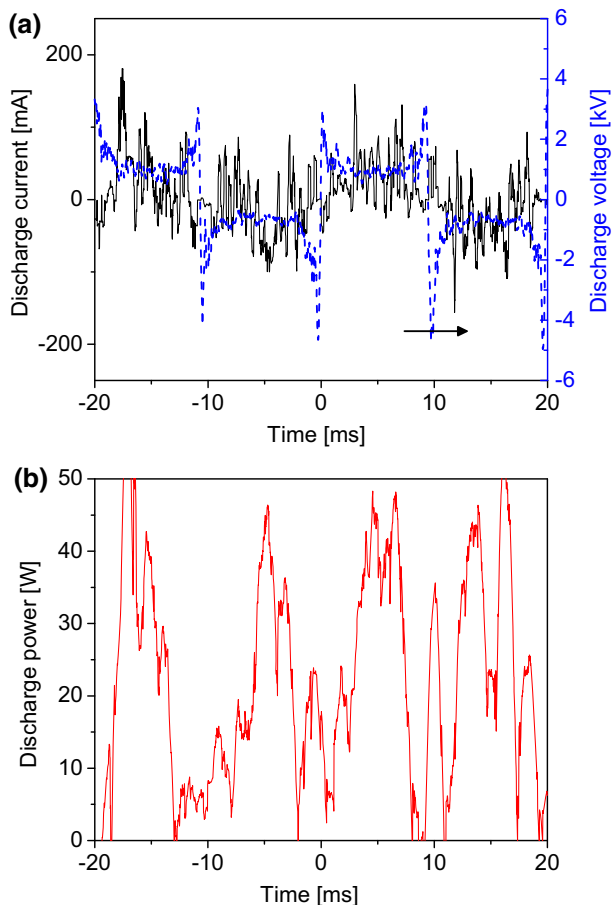


Fig. 1 Schematic of the device showing several dimensions. Also the jet electric circuit is shown

ballasts was not necessary. The discharge current was inferred from the measurement of the voltage drop across a shunt resistor ($100\ \Omega$) connected in series with the discharge, while the discharge voltage was measured by using a high-impedance voltage probe (Tektronix P6015A, 1000X, 3pf, $100\ \text{M}\Omega$). Both electrical signals were simultaneously registered by using a 4-channel oscilloscope (Tektronix TDS 2004C with a sampling rate of 1 GS/s and an analogical bandwidth of 70 MHz).

The discharge voltage $U(t)$, together with the discharge current $i(t)$ are shown in Fig. 2a, while the time-resolved power deposition inside the discharge chamber is presented in Fig. 2b. The discharge current exhibits multiple sharp spikes (because of development of ionization instabilities in the plasma) of relative large amplitude superimposed on a sinusoidal profile (with a frequency of 50 Hz); almost independent of the discharge characteristics; since the current amplitude is controlled by the transformer impedance. The voltage signal also has a frequency of 50 Hz and decreases when the current increases; thus leading to a negative slope in the voltage–current characteristic of the discharge. All these features suggest that this discharge regime may be considered to be a high-pressure glow-type discharge operating in constricted (filamentary) mode [30, 31]. The jet operating power was calculated as:

Fig. 2 Waveforms of **a** discharge voltage and current and **b** power deposition under the jet operating conditions



$$P = \frac{1}{\tau} \int i(t) U(t) dt, \tag{1}$$

where τ is the discharge period. The resulting power was about 22 W. As it is well known, only a fraction of the discharge power is expended in heating the gas, while an important remaining part of this power is dissipated by thermal conduction and several processes on the electrode sheaths (typically the cathode in this case). Since this is a very short discharge in the axial direction (~ 1 mm), the heat conduction to the electrodes dominates over the radial conduction, and typically takes about 50% of the deposited power (e.g., [32]). So, including the surface electrode losses, it can be safely assumed that about 40% of the power deposition is available for heating the gas flow through convection. Considering that the transit time of a volume element of gas through the discharge ($\sim 10^{-4}$ s) is very short as compared to the power deposition period (with a main frequency of 100 Hz as it is shown in Fig. 2b), it can be inferred from the instantaneous power values given in Fig. 2b, that the gas temperature at the nozzle exit should presents a 100 Hz oscillation with a maximum value of about 420 K and an average value close to 350 K; for the typical gas mass flow values of this experiment.

Optical System

A parallel-beam mirror schlieren system was used in this research. As the parabolic mirrors ($\lambda/8$, 152 mm in diameter) were not identical, a typical (coma free) Z-system [13, 14] could not be employed. Figure 3 shows a schematic of the chosen experimental setup. In order to minimize the coma aberration of the system (the coma aberration grows in proportion to the offset angle and to the inverse square of the mirror f/no —for a given offset angle—[13]); the offset angle of the second parabolic mirror ($f/2$) was reduced to zero by mounting the light sensor (camera) on the optical axis of the second branch of the system. In spite of the fact that this configuration blocked a considerable part of the center of the test region, the effluent of the plasma jet was successfully investigated with the peripheral zone of the field. Also to reduce both astigmatism and coma, the offset angle of the first parabolic mirror ($f/8$) was restricted to its minimum practical value. With all of these

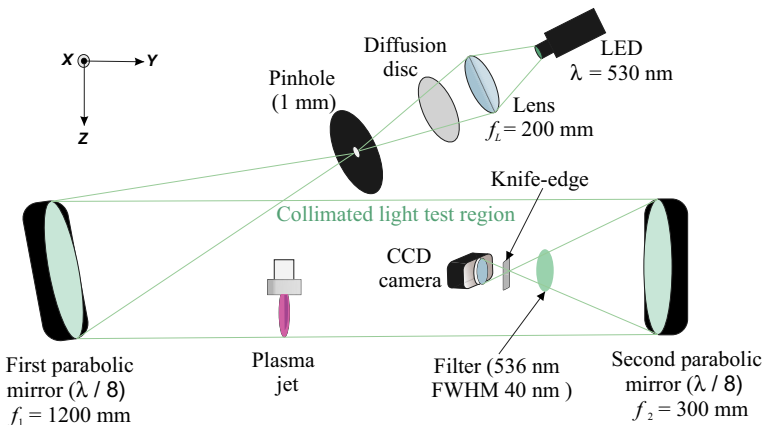


Fig. 3 Optical system

precautions, a uniform darkening of the schlieren image at the exit focal plane of the optical system was obtained as the knife-edge was advanced.

The point light source was constructed by focusing the light from a green LED (dominant wavelength 530 nm) through a best-form lens (focal length 200 mm) on a pinhole with 1.0 mm diameter. Between the focusing lens and the pinhole, a diffusion disc was placed in order to achieve a homogeneous lighting in the test region. The pinhole was placed in the focal point of the first parabolic mirror ($f_1 = 1200$ mm), which creates the collimated light test region of the schlieren system. After passing through the test region in which the plasma jet was placed, the collimated light was again focused by the second parabolic mirror ($f_2 = 300$ mm) onto the knife-edge plane. The knife-edge (positioned parallel to the z direction) was adjusted so that the detected intensity signal was approximately $\sim 48\%$ of the signal without the knife edge. A band-pass filter centered in a wavelength of 530 nm with a full width at half maximum FWHM of 40 nm (placed between the second parabolic mirror and the knife edge) was used to block the light emitted from the plasma jet. The schlieren images (with a size of 640×480 pixels) were acquired with a charge-coupled device Lumenera digital camera with an exposure time of 80 ms. These images were stored in BMP format and digitized by an 8-bit gray-level frame grabber. According to the magnification of this optical system, the spatial resolution in the schlieren image was about ~ 0.036 mm (36 pixels corresponded to 1 mm).

In addition to the quantitative schlieren diagnostics, the average gas temperature was also measured using a k-type thermocouple located inside the plasma jet.

Experimental Results and Discussion

Kinetic Model of the Effluent

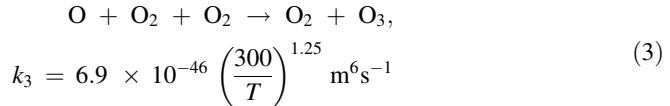
Schlieren visualization of plasma jet is based on the fact that the plasma represents a transparent medium for the LED light (i.e., the light frequency \gg plasma frequency). As for every optical medium, the refractivity ($n-1$, being n the refraction index of the medium) is the characteristic parameter. Since for a given wavelength of illumination n depends on the plasma composition and its density or pressure, the measurement of the plasma jet refractivity leads to conclusions on those plasma parameters. The plasma refraction index (at a given wavelength) can be described for the Lorenz-Lorentz equation [14],

$$\frac{n^2 - 1}{n^2 + 2} = \frac{4\pi}{3} N \sum_i x_i \alpha_i, \quad (2)$$

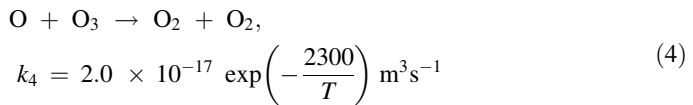
where N is the gas particle density, and α_i and x_i represents the mean polarizability and the molar fraction of species i ; respectively. The plasma polarization depends both on the bound and the free electrons [14]. However, the influence of the free electrons becomes important only at ionization degrees of a few percent. Because the electron densities in the effluent of atmospheric-pressure non-thermal plasma jets are of the order of 10^{15} – 10^{17} m^{-3} (depending on the experimental conditions and the specific point in the jet) [1]; the contribution of the free electrons was neglected. Furthermore, the contribution of the ionized species was also neglected (the ion refractivity can in general be neglected as compared with the electron refractivity since both densities are the same [12]). With regard to the contribution of the excited states to the plasma refractive index, their influence can also be

ignored in the visible region of the spectrum because in the studied gas (and also in air [24], argon [29] and other gases); the resonance spectral lines are situated in the vacuum ultraviolet region of the spectrum [12]. The contribution of other reactive particles as O and O₃ deserves a discussion.

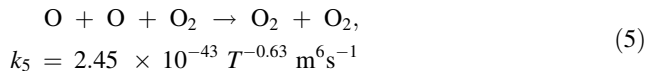
In the effluent, almost all O atoms produced in the glow discharge region are rapidly converted into ozone [1, 2], since the O association with O₂ through the three-body reaction,



at low-gas temperatures (close to room temperature) is much faster than the reactions,

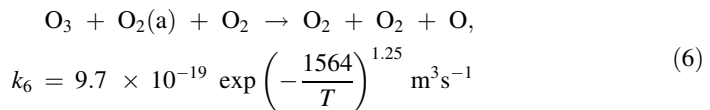


and



The rate coefficients k_3 – k_5 were taken from [33]. T is the gas temperature. Under the present conditions, more than 99% of the atomic oxygen is converted into O₃ through reaction (3) during a time of $\Delta t \approx 10 \mu\text{s}$ (i.e., at a distance $z = u \Delta t \approx 2 \text{ mm}$ from the nozzle exit, being u the mean gas flow velocity in the jet outflow). Note that the length-scale for diffusive losses ($D \Delta t$)^{1/2} (being $D = 0.27 \times 10^{-4} \text{ m}^2/\text{s}$ the diffusion coefficient of the ground state atom O(³P) at room temperature [34]) is much shorter than 1 mm; so that diffusion phenomena are not relevant in this conditions. Therefore, except in the near field of the outflow ($z < 2 \text{ mm}$), the density of the atomic oxygen can be neglected; instead, the presence of the ozone should be considered there.

It should be noted that the atomic oxygen can be also created in the far field by collisions between the molecular metastable O₂(a) and O₃ through the reaction [1, 2],



however, the rate coefficient [33] of reaction (6) is quite low at room temperature; thus explaining why O₂(a) and O₃ are long living species as compared with the typical time-scale (10^{-4} – 10^{-1} s) of the gas movement along the jet.

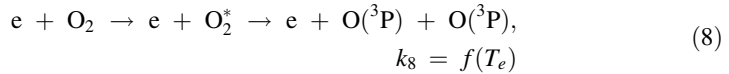
Notice that the discussion of the chemistry in the jet outflow was based on the assumption that the gas temperature is near room temperature. Since the chemistry considered occurs on a fast timescale (e.g. microseconds), the relevant gas temperature could be substantially higher than the (time-averaged) measured values. Not only the low-frequency fluctuation of the input power, but also the temporal averaging arising from the procedure itself (the turbulent flow was measured on timescales much larger than the

Kolmogorov-timescale) can cause deviations from the real instantaneous value of the gas temperature at a given point in the jet outflow.

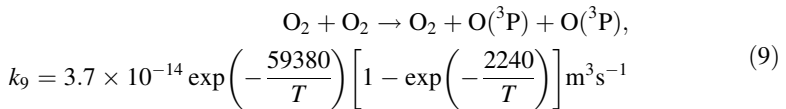
The O density at the nozzle exit was estimated as:

$$2 \times k_8 [\text{O}_2] N_e \tau_{\text{flow}}, \quad (7)$$

where τ_{flow} is the transit time of the gas through the discharge and k_8 is the rate coefficient of the electron-impact dissociation reaction,



being O_2^* the pre-dissociative excited state of O_2 with an energy threshold of 6 eV [35, 36]. The rate coefficient k_8 was evaluated as a function of the effective electron temperature T_e by solving the electron Boltzmann equation with the help of the BOLSIG+ code [37]. In (7) the density of the heavy particles is denoted by square brackets and the density of electrons by N_e . Note that (7) actually represents the upper-limit of the O density at the near field of the outflow as recombination processes were neglected there. Note also that the thermal dissociation of O_2 through the reaction,



(being the rate coefficient k_9 taken from [38]) does not play a relevant role because the gas temperature in the glow discharge region is not high-enough ($\sim 1000\text{--}2000$ K, on the basis of measured values [39, 40]). Being $N_e \sim 10^{18}\text{--}10^{19} \text{m}^{-3}$ and $T_e \sim 0.8\text{--}1$ eV (which are typical values for atmospheric-pressure glow-type discharges in molecular gases at current levels of 10–200 mA [30, 41, 42]) and $\tau_{\text{flow}} \sim 10^{-4}$ s (the characteristic length scale of the discharge is 1 mm, while the gas flow velocity in the inter-electrode gap is around 10 m/s), the $\text{O}({}^3\text{P})$ density at the nozzle exit results $\sim 1 \times 10^{20} \text{m}^{-3}$; thus corresponding to a relatively low dissociation degree of about 2×10^{-6} .

The estimated atomic oxygen density can be compared with the numerical results in a non-thermal atmospheric-pressure glow discharge (200 mA) in a preheated (2200 K) air flow [41]. For a transit time of the gas through the discharge of 100 μs , an atomic oxygen density of about $4 \times 10^{20} \text{m}^{-3}$ (corresponding to a dissociation degree of about 6×10^{-5}) was found. The difference being attributed to the enhancement of the high-energy threshold processes involving electrons owing to superelastic collisions with vibrationally-excited nitrogen molecules; and also due to the dissociation of excited electronic states of oxygen molecules that are produced during the quenching of the electronic excited states of N_2 molecules [35, 36, 41].

$\text{O}({}^3\text{P})$ density measurements in an atmospheric-pressure plasma jet operating at room temperature (with an rf power level of $\sim 10\text{--}25$ W) with noble gases containing small admixtures of O_2 were reported [43]. The results shown that the O atom density in the near field of the effluent increases with a steep slope with an increasing amount of O_2 in the plasma up to a maximum of $2 \times 10^{20} \text{m}^{-3}$ at about 0.6% O_2 admixture (i.e., an oxygen dissociation degree of about 7×10^{-4}). Beyond this value, the O density decreases with the increase of the O_2 admixture. The reason of that is related to the fact that large concentration of molecules significantly changes the energy distribution function of the

electrons (due to rotational and vibrational molecular excitations); thus reducing the amount of the electron energy which can be used for the oxygen dissociation [1, 43].

Calculations performed on the basis of the estimated value of dissociation at the nozzle exit yield a negligible error (much less than 1 K) in the derivation of the gas temperature in the whole field of the outflow. An atomic oxygen polarizability $\alpha(\text{O}) = 0.77 \text{ \AA}^3$ for a wavelength of 480 nm [44] and an ozone polarizability $\alpha(\text{O}_3) = 3.06 \text{ \AA}^3$ for a wavelength 589 nm [14], was used. Furthermore, estimations show that the gas temperature measurement is not seriously affected by the ozone density up to oxygen dissociation degrees of at least 10^{-3} (i.e., an atomic oxygen density $\sim 10^{23} \text{ m}^{-3}$ under the conditions considered). As quoted before, since almost all O atoms produced in the enclosed discharge are rapidly converted into ozone in the near-field of the jet outflow, an ozone density of about $2 \times 10^{23} \text{ m}^{-3}$ would result in a maximum error of only 2–3 K; being in this case the uncertainty in the temperature nearly equal to that derived from a 10% change in the average oxygen molar fraction when the penetration of the ambient air into the effluent (due to turbulent diffusion) was taken into account.

Data Processing

For gases the refraction index $n \approx 1$, therefore (2) becomes the so called Gladstone–Dale relation [13, 14],

$$n - 1 = \frac{N_r}{N_r} \sum_i x_i (n - 1)_{i,r} = \frac{p T_r}{p_r T} \sum_i x_i (n - 1)_{i,r}, \quad (10)$$

being $(n-1)_{i,r}$ the reference refractivity for species i at density N_r . Note that in the second equality in (10) the density was replaced by the pressure p and the gas temperature T by using the ideal gas law. Apart from the wavelength, the refractive index of air depends on the temperature. The room temperature was measured to be $T_r \approx 293 \text{ K}$. For the calculation of the air refractive index the web application provided by National Institute for Standards and Technology NIST [45] was used and yields $(n-1)_{\text{air},r} = 2.713 \times 10^{-4}$. For oxygen a refractivity $(n-1)_{\text{o},r} = 2.567 \times 10^{-4}$ for a wavelength 546 nm was used [46].

It is well known that when a light ray passes through a non-homogeneous medium, it suffers a deviation in its trajectory by a certain angle ε that depends both, on the refractive index gradient and on the thickness of the medium under test. Such ray path deviations through a non-homogeneous medium is expressed as [13],

$$\varepsilon_\xi = \int \frac{1}{n} \frac{dn}{d\xi} dy, \quad (11)$$

where y is the optical axis direction (see Fig. 3) and ξ can be either x or z coordinate, depending on the direction in which the knife blocks out the light. Since in this work the knife-edge was positioned parallel to the z direction, the analysis was done for the x direction (i.e., visualizing only the x -component of the refractive index gradient of the jet) When the measuring range of the schlieren system has not been exceeded [13, 14], the contrast C of the light pattern on the schlieren image (defined as the ratio of the differential illuminance at a given image pixel to the value of its background level illuminance) is the output of the schlieren system. As the parallel light beam passes the test region in y -direction, the signal is integrated in y -direction. By assuming circular symmetry in the plasma jet, the contrast is given by [13, 14]:

$$C \equiv \frac{I - I_k}{I_k} \approx 2S \frac{\partial}{\partial x} \int_0^{\infty} n(r) dy, \quad (12)$$

where the last approximation in (12) follows from the fact that n is quite close to unity. I is the intensity measured on the schlieren image with the reference schlieren object in the test region, I_k is the reference intensity (without any schlieren object); but with the knife edge inserted, r is the radial coordinate (measured from the jet axis) and S ($\equiv \partial C/\partial \varepsilon$) [13] the sensitivity of the schlieren system.

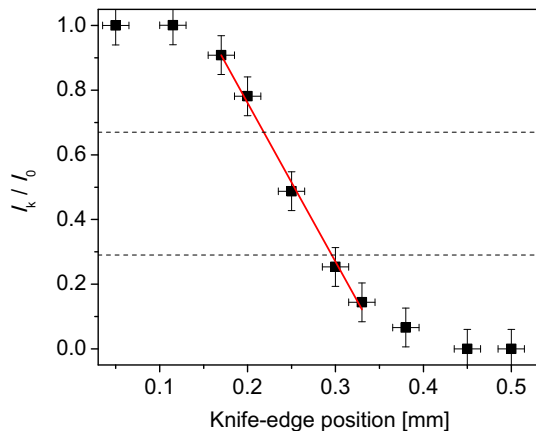
A calibration was performed without the schlieren object to find the relation between the contrast C and the deflection angle ε_x . The procedure consisted in measuring I_0 without the knife-edge mounted and then measuring I_k as a function of the knife-edge position (x) and normalizing I_k by I_0 . The result is shown in Fig. 4. As expected, the use of a circular aperture leads to a non-linear behavior, but only for I_k/I_0 near 0 and 1. As in the present experiment the intensity ratio was measured to be $I_k/I_0 = 0.48$, and the contrast in all experiments $C \leq 0.4$ was small enough (see below); the background illumination level was linear with respect to the degree of the knife-edge cutoff (the measuring range is indicated by dashed lines in Fig. 4). Recalling the definition of contrast given by (12) and expanding I_k/I_0 to first order in x , the sensitivity of the schlieren system can be determined from the slope of the linear part of the calibration curve (indicated with a red line in Fig. 4) as:

$$S \approx f_2 \frac{d(I_k(x)/I_0)/dx}{I_k(x)/I_0}, \quad (13)$$

where the approximation for small angles ($\Delta x \approx f_2 \varepsilon_x$) was used. For the present conditions the sensitivity of the experiment was calculated to be $S = 3000 \pm 300$. The relative large error value in the sensitivity of the system is due to the strong dependence of the sensitivity on the knife-edge position x , thus small errors significantly affect the obtained densities and temperatures results. However, as the molar fraction of oxygen at the nozzle exit is known to be $x_{O_2} = 1$, the sensitivity of the schlieren system was fitted so that $x_{O_2} = 1$ close to the nozzle exit. This calibration method proved to be more accurate than the direct calculation of the sensitivity according to (13).

Using the experimental C data and the Abel inversion technique [12], (12) can be inverted to obtain the radial profile (for a given z value) of the effluent refraction index,

Fig. 4 Image illumination as a function of the knife-edge position



$$n(r) - n(\infty) = -\frac{1}{S} \int_r^{\infty} \frac{C(x)}{\pi(x^2 - r^2)^{1/2}} dx, \quad (14)$$

being $n(\infty)$ the refraction index of the surrounding medium (air). Note that (14) does not require any differentiation of the experimental data $C(x)$. This turns out to be one of the major advantages of schlieren techniques over interferometry [26]. Finally, replacing the Eq. (10) in (14), the time-averaged gas temperature of the plasma jet can be calculated from:

$$T(r) = T_r \frac{\sum_i x_i (n - 1)_{i,r}}{n(\infty) - 1 - \frac{1}{S} \int_r^{\infty} \frac{C(x)}{\pi(x^2 - r^2)^{1/2}} dx}. \quad (15)$$

The precise determination of the gas temperature of the plasma jet through (15) requires the previous knowledge of the time-averaged molar fraction of the oxygen in the jet. If the flow regime does not change from laminar to turbulent when the discharge is turned on (i.e., if the diffusion phenomena does not significantly changes), this can be achieved by measuring the contrast when only the gas flow is turned on (but the plasma is not ignited); by assuming some hypothesis about the thermodynamic state of the gas. The simplest assumption of an isothermal flow was assumed [29]. Gas temperature measurements inside the jet (when the discharge is off) by using a thermocouple supported such an assumption. Therefore, the time-averaged molar fraction of the oxygen was calculated from the gas contrast by assuming $T = T_r$. Then, the discharge was turned on and the plasma contrast was measured to calculate the gas temperature.

Under the present experimental conditions the Reynolds number (based on the scale length given by the nozzle-hole diameter) was about 13,800. As this number is greater than 3000 [47], the jet has a fully turbulent structure (regardless the presence of the discharge). The constancy of the cone angle of the jet between the discharge off (Fig. 5a) and the discharge on (Fig. 5b) cases also reinforces this assumption. The non-influence of the discharge on the cone angle of the jet can also be better observed by comparing the contrast radial profiles (at a given axial distance from the nozzle exit) obtained with the discharge off (Fig. 6a) and when the discharge is turned on (Fig. 6b). In this situation, the effective diffusion coefficient is obtained by adding to the molecular diffusion coefficient, a turbulent one,

$$D_t \approx 0.009 du, \quad (16)$$

being d the nozzle-hole diameter and u the mean-velocity of the gas flow at the nozzle exit [32]. Since $D_t \approx 1.9 \times 10^{-3} \text{ m}^2/\text{s}$ is two orders of magnitude greater than the oxygen molecular diffusion coefficient ($=0.187 \times 10^{-4} (T/300)^{3/2} \text{ m}^2/\text{s}$) for $T \approx 300\text{--}400 \text{ K}$ [48]; the diffusion phenomena in the jet only depends on the gas flow velocity. As the gas pressure at the inlet of the jet device was kept constant during the experiments, the momentum of the jet ($\sim N u^2$) does not vary during the discharge ignition. Therefore, an absolute difference of 20% in the gas density (or in the temperature, as the results show) produced only a 10% of change in the gas flow velocity; yielding a similar change in the average oxygen molar fraction of the jet. Such a difference of 10% would result in a maximum error less than 2 K according to Eq. (15).

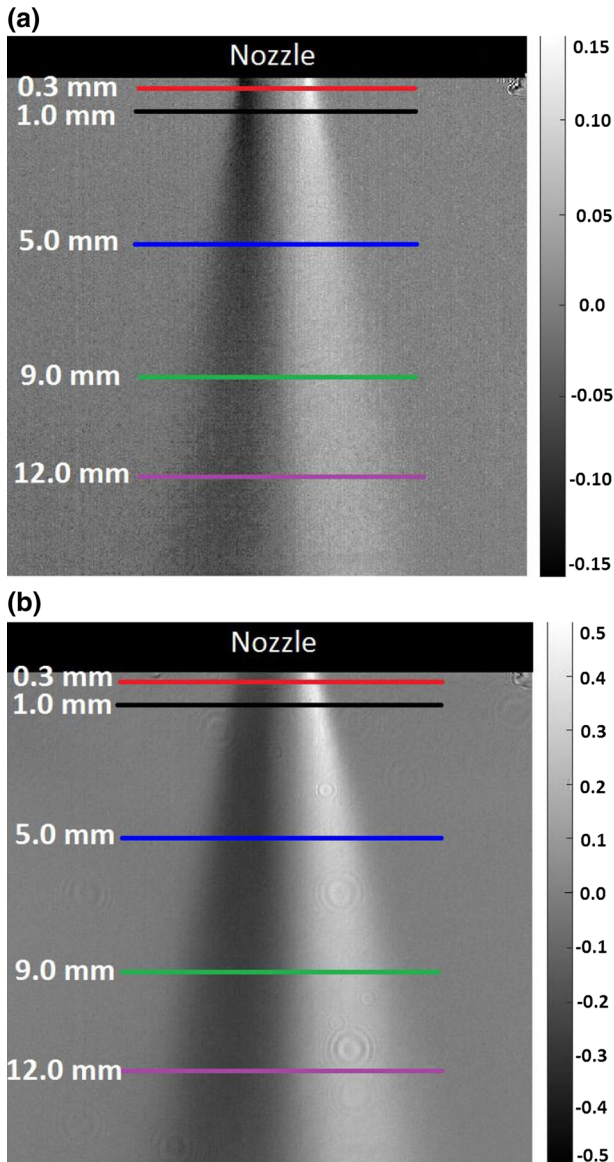


Fig. 5 Schlieren image contrast obtained for an oxygen gas flow of 10 NI/min **a** with the discharge off and **b** when the discharge is turned on

In order to determine the contrast of a schlieren image, the intensity I for each pixel was measured for the discharge on and discharge off cases and then its difference with the background light intensity I_k , normalized by I_k . The relative time-averaged intensities were obtained by averaging 10 images, each captured with an exposure time of 80 ms. Figure 5 shows both (time-averaged) contrasts for the gas flow (a) when the discharge is turned off and (b) when the discharge is turned on (plasma jet).

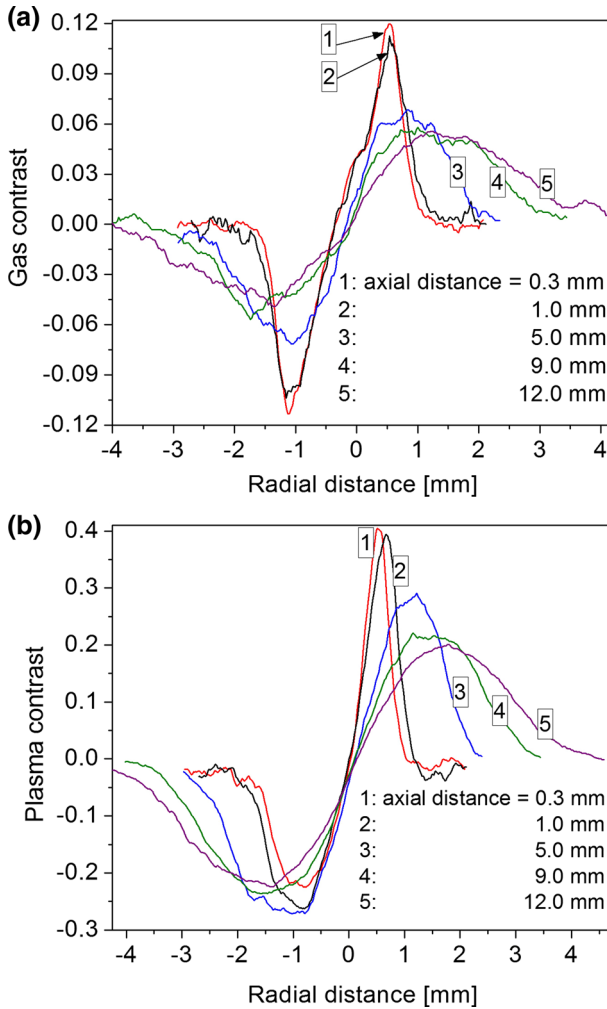


Fig. 6 Contrast radial profiles along the lines shown in Fig. 5 obtained **a** without the discharge and **b** when the discharge is turned on

In Fig. 6 the contrast radial profiles along the lines indicated in Fig. 5 obtained for an oxygen gas flow of 10 NI/min (a) with the discharge off and (b) when the discharge is turned on are shown. The profiles shown in Fig. 6a demonstrates that the signal in the plasma off case is quite symmetric, both in the near and in the far field of the outflow. However in the plasma on case, showed in Fig. 6b, relative strong departures from the symmetry are evident in the near field. As expected, in the far field (at distances larger than 5 mm from the nozzle exit) the asymmetry vanishes. These results suggest that the asymmetry in the plasma contrast profiles is caused by the presence of the discharge itself inside the jet device. For the plasma jet operating conditions a filamentary glow-type discharge in a gas flow with relatively high-gas temperature ($\sim 1000\text{--}2000\text{ K}$) [39–41, 49] likely exists in the inter-electrode gap. It can be expected, therefore, that the cold-gas streamlines entering the high-temperature zone become tilted as they undergo refraction in

the layer where the temperature abruptly increases (because of the expansion of the gas upon heating); thus causing local asymmetries in the plasma flow (which rapidly vanish in the far field due to diffusive processes).

Results

Previous to applied the Abel inversion procedure (to find the radial profiles of the oxygen molar fraction and gas temperature), the contrast data were smoothed (by taken an arithmetic average of subsequences of ~ 10 terms) and then interpolated with a high-order polynomial function to keep the errors to a minimum. The results of the inversion are shown in Figs. 7, 8 and 9. Figure 7 shows the time-averaged radial profiles (along the lines indicated in Fig. 5) of the oxygen molar fraction obtained by the schlieren measurement. As quoted before, the experimental sensitivity S was fitted so that the oxygen molar fraction was 1 at the nozzle exit. The sensitivity obtained in this way gave a value $S \approx 3049$ (which coincides within the experimental error with the S value obtained from the calibration curve). As expected, the inferred profiles of the oxygen molar fraction drop more gently in the far field since they are governed by diffusion phenomena. As it can be seen, the air rapidly penetrates the plasma jet reaching a molar fraction of 25% 12 mm away from the nozzle exit. This is also showed in Fig. 9. The uncertainty in the molar fraction measurements (within 10%) was primarily from errors associated to the Abel inversion procedure through some asymmetry of the gas contrast field.

Figure 8 shows the time-averaged radial profiles (along the lines indicated in Fig. 5) of the plasma jet gas temperature obtained by the schlieren measurement; while the axial profile but with a finer resolution in the near-field of the jet outflow is shown in Fig. 9. According to what was discussed in the Experimental arrangement Section, this temperature values represent a temporally averaged values of a gas temperature which should perform a 100 Hz oscillation between the ambient value and a maximum of about 420 K.

As expected, the time-averaged gas temperature of the jet was near to the room value with a maximum departure of about 55 K. The uncertainty in the temperature measurements was within 6 K. (mainly from errors associated to the Abel inversion procedure through the asymmetry of the plasma contrast in the near field and the above uncertainty in the molar fraction radial profiles). It is worth to noting that in the Abel inversion of the

Fig. 7 Radial profiles of the oxygen molar fraction along the lines shown in Fig. 5

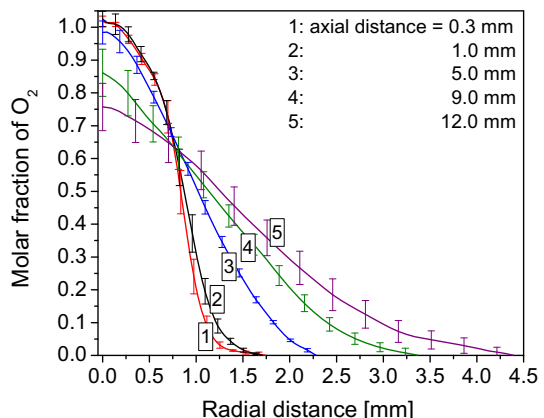


Fig. 8 Radial profiles of the gas temperature of the plasma jet along the lines shown in Fig. 5

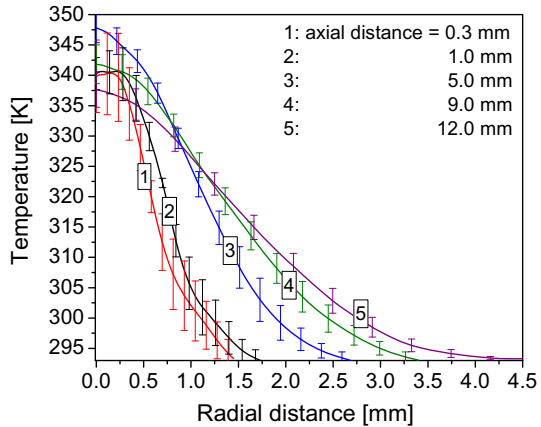
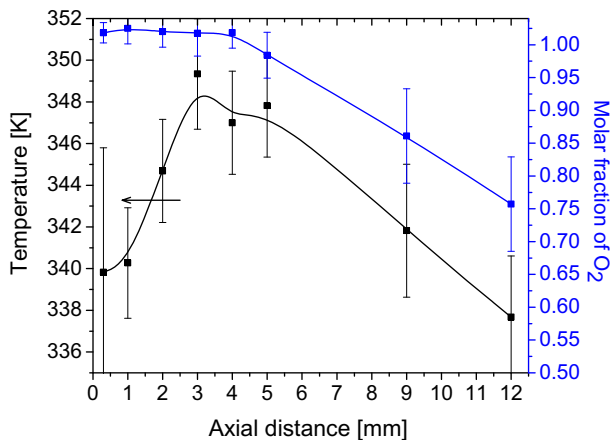


Fig. 9 Axial profiles of the gas temperature of the plasma jet and oxygen molar fraction



contrast, values obtained for a specific radial position depend on all the data obtained for radii larger than such a specific position; therefore, small deviations may therefore add up towards the axis.

The point that for low-gas temperatures the change of the index of refraction due to the mixing of the working gas and the air is in the same order of magnitude as the change due to the gas temperature is not problematic provided that the flow regime does not change from laminar to turbulent when the plasma is turned on. On the contrary, the gas flux (with plasma turned off) can be used to precisely calibrate the system in the sensitivity region of interest [29].

Also thermocouple measurements with a low-spatial resolution (~1 mm) at ~3 mm from the nozzle exit were performed. While a deviation between both techniques was expected as the probe was probably perturbing the plasma (owing to its finite size), the thermocouple measurements showed good agreement with the schlieren measurements (within 5 K).

The results showed an increase in the gas temperature of about 8 K in the region between 0 and ~5 mm away from the nozzle exit. These results suggest that in the near field some gas heating still occurs. It is worth noting that this increase is not related to any

heating process inside the discharge chamber, but, because of the high-gas heating rate value ($\partial T/\partial t \approx u \partial T/\partial z \approx 0.3 \text{ K/ms}$) associated with this phenomenon, it would be a consequence of several fast gas heating mechanism [50, 51] resulting from the energy release during the quenching of the long-lifetime electronically excited particles dragged by the gas flow from the enclosed discharge. The electron-ion recombination heating could also play a role. The same behavior was previously reported but for a non-thermal atmospheric-pressure argon plasma jet [29]. Both experimental and numerical work would be needed to clarify such a point.

Conclusions

A quantitative interpretation of the schlieren technique applied to a non-thermal atmospheric-pressure oxygen plasma jet driven at low-frequency (50 Hz) was reported. The jet was operated in the turbulent regime, with a hole-diameter based Reynolds number of 13,800. The calibration of the optical system was obtained by fitting the sensitivity parameter so that the oxygen fraction at the nozzle exit was unity. The results have shown that:

1. The radial profiles of the contrast in the discharge off case were quite symmetric in the whole outflow, but in the discharge on case, relative strong departures from the symmetry were evident in the near field. These results suggest that the (high-gas temperature) filamentary glow-type discharge inside the jet device cause local asymmetries in the plasma flow which rapidly vanish in the far field due to diffusive processes.
2. The gas temperature of the jet was near to the room value, with a maximum departure of about 55 K. The inferred temperature values represent temporally averaged values of a gas temperature which should perform a 100 Hz oscillation between the ambient value and a maximum of about 420 K. The penetration of the ambient air into the jet due to turbulent diffusion was taken into account. The uncertainty in the temperature measurements was within 6 K, primarily derived from errors associated to the Abel inversion procedure.
3. The results showed an increase in the gas temperature of about 8 K in the region between 0 and 5 mm away from the nozzle exit. The same behavior was previously reported but for a non-thermal atmospheric-pressure argon plasma jet. These results suggest that some gas heating still occurs in the near field of the outflow. Both experimental and numerical work would be needed to clarify such a point.

Acknowledgements This work was supported by Grants from the CONICET (PIP 11220120100453), Universidad Tecnológica Nacional (PID 2264 and PID 4626) and ANPCyT (PICT 2015-1553). L. P. is a member of the CONICET. J. C. C. and E. C. thank CONICET for their doctoral fellowships.

References

1. Lua X, Naidis GV, Laroussi M, Reuter S, Graves DV, Ostrikov K (2016) *Phys Rep* 630:1–84
2. Graves DB (2014) *Phys Plasmas* 21:080901
3. Staack D, Farouk B, Gutsol A, Fridman A (2007) *Plasma Sources Sci Technol* 17:025013
4. Kunhardt EE (2000) *IEEE Trans Plasma Sci* 28:189–200
5. Fridman A, Chirokov A, Gutsol A (2005) *J Phys D Appl Phys* 38:R1–R24

6. Park GY, Park SJ, Choi MY, Koo IG, Byun JH, Hong JW, Sim JY, Collins GJ, Lee JK (2012) *Plasma Sources Sci Technol* 21:043001
7. Laroussi M, Kong MG, Morfill G, Stolz W (2012) *Plasma medicine*, vol 1. Cambridge University Press, Cambridge
8. Walsh JL, Kong MG (2011) *Appl Phys Lett* 99:081501
9. Pei X, Lu X, Liu J, Liu D, Yang Y, Ostrikov K, Chu PK, Pan Y (2012) *J Phys D Appl Phys* 45:165205
10. Yan W, Han ZJ, Liu WZ, Lu XP, Phung BT, Ostrikov K (2013) *Plasma Chem Plasma Process* 33:479–490
11. Minotti F, Giuliani L, Xaubert M, Grondona D (2015) *Phys Plasmas* 22:113512
12. Ovsyannikov AA, Zhukov MF (2005) *Plasma diagnostics*. Cambridge International Science Publishing, Cambridge
13. Settles GS (2001) *Schlieren and shadowgraph techniques*. Springer, Berlin
14. Vasilev LA (1971) *Schlieren methods*. Keter Inc., New York
15. Jiang N, Yang J, He F, Cao Z (2011) *J Appl Phys* 109:093305
16. Oh JS, Olanbani OT, Hale C, Mariani R, Kontis K, Bradley JW (2011) *J Phys D Appl Phys* 44:155206
17. Bradley JW, Oh JS, Olanbani OT, Hale C, Mariani R, Kontis K (2011) *IEEE Trans Plasma Sci* 39:2312–2313
18. Ghasemi M, Olszewski P, Bradley JW, Walsh JL (2013) *J Phys D Appl Phys* 46:052001
19. Robert E, Sarron V, Darny T, Ries D, Dozias S, Fontane J, Joly L, Pouvesle JM (2014) *Plasma Sources Sci Technol* 23:012003
20. Boselli M, Colombo V, Ghedini E, Gherardi M, Laurita R, Liguori A, Sanibondi P, Stancampiano A (2014) *Plasma Chem Plasma Proc* 34:853–869
21. Kelly S, Golda J, Turner MM, Schulz-von der Gathen V (2015) *J Phys D Appl Phys* 48:444002
22. Zheng Y, Wang L, Ning W, Jia S (2016) *J Appl Phys* 119:123301
23. Qaisrani MH, Xian Y, Li C, Pei X, Ghasemi M, Lu X (2016) *Phys Plasmas* 23:063523
24. Xu DA, Shneider MN, Lacoste DA, Laux CO (2014) *J Phys D Appl Phys* 47:235202
25. Alvarez-Herrera C, Moreno-Hernández D, Barrientos-García B (2008) *J Opt A: Pure Appl Opt* 10:104014
26. Kogelschatz U, Schneider WR (1972) *Appl Opt* 11:1822–1832
27. Prevosto L, Artana G, Mancinelli B, Kelly H (2010) *J Appl Phys* 107:023304
28. Prevosto L, Artana G, Kelly H, Mancinelli B (2011) *J Appl Phys* 109:063302
29. Schmidt-Bleker A, Reuter S, Weltmann KD (2015) *J Phys D Appl Phys* 48:175202
30. Akishev Y, Grushin M, Karalnik V, Petryakov A, Trushkin N (2010) *J Phys D Appl Phys* 43:075202
31. Prevosto L, Kelly H, Mancinelli B, Chamorro JC, Cejas E (2015) *Phys Plasmas* 22:023504
32. Raizer YuP (1991) *Gas discharge physics*. Springer, Berlin
33. Kossyi IA, Kostinsky AY, Matveyev AA, Silakov VP (1992) *Plasma Sources Sci Technol* 1:207–220
34. Yolles RS, Wise H (1968) *J Chem Phys* 48:5109–5115
35. Aleksandrov NL, Kindysheva SV, Nudnova MM, Starikovskiy AY (2010) *J Phys D Appl Phys* 43:255201
36. Popov NA (2011) *J Phys D Appl Phys* 44:285201
37. Hagelaar GJM, Pitchford LC (2005) *Plasma Sources Sci. Technol.* 14:722–733. Freeware code BOLSIG + version 07/2015. www.bolsig.laplace.univ-tlse.fr (2015)
38. Aleksandrov NL, Bazelyan EM, Kochetov IV, Dyatko NA (1997) *J Phys D Appl Phys* 30:1616–1624
39. Xiao D, Cheng C, Shen J, Lan Y, Xie H, Shu X, Meng Y, Li J, Chu PK (2014) *Phys Plasmas* 21:053510
40. Xiao D, Cheng C, Shen J, Lan Y, Xie H, Shu X, Meng Y, Li J, Chu PK (2014) *J Appl Phys* 115:033303
41. Popov NA (2006) *Plasma Phys Rep* 32:237–245
42. Prevosto L, Kelly H, Mancinelli B (2016) *Plasma Chem Plasma Proc* 36:973–992
43. Knake N, Reuter S, Niemi K, Schulz-von der Gathen V, Winter J (2008) *J Phys D Appl Phys* 41:194006
44. Alpher RA, White DR (1959) *Phys Fluids* 2:153–161
45. National Institute of Standards and Technology. Engineering metrology toolbox. <http://emtoolbox.nist.gov/Wavelength/Ciddor.asp>. Last updated Nov 2004
46. Weber MJ (2002) *Handbook of optical materials*. CRC Press, Boca Raton
47. Ungate CD, Harleman DR, Jirka GH (1975) Stability and mixing of submerged turbulent jets at low Reynolds numbers. MIT Energy Lab Rep
48. Weissman S, Mason EA (1962) *J Chem Phys* 37:1289–1300
49. Yu L, Laux CO, Packan DM, Kruger CH (2002) *J Plasma Phys* 91:2678–2686
50. Boeuf JP, Kunhardt EE (1986) *J Appl Phys* 60:915–923
51. Mintousov EI, Pendleton SJ, Gerbault FG, Popov NA, Starikovskaia SM (2011) *J Phys D Appl Phys* 44:285202